

sMRI-PatchNet: A novel explainable patch-based deep learning network for Alzheimer's disease diagnosis and discriminative atrophy localisation with Structural MRI

Xin Zhang, Liangxiu Han*, Lianghao Han, Haoming Chen, Darren Dancey, Daoqiang Zhang

Abstract—Structural magnetic resonance imaging (sMRI) can identify subtle brain changes due to its high contrast for soft tissues and high spatial resolution. It has been widely used in diagnosing neurological brain diseases, such as Alzheimer's disease (AD). However, the size of 3D high-resolution data poses a significant challenge for data analysis and processing. Since only a few areas of the brain show structural changes highly associated with AD, the patch-based methods dividing the whole image data into several small regular patches have shown promising for more efficient sMRI-based image analysis. The major challenges of the patch-based methods on sMRI include identifying the discriminative patches, combining features from the discrete discriminative patches, and designing appropriate classifiers. This work proposes a novel patch-based deep learning network (sMRI-PatchNet) with explainable patch localisation and selection for AD diagnosis using sMRI. Specifically, it consists of two primary components: 1) A fast and efficient explainable patch selection mechanism for determining the most discriminative patches based on computing the SHapley Additive exPlanations (SHAP) contribution to a transfer learning model for AD diagnosis on massive medical data; and 2) A novel patch-based network for extracting deep features and AD classification from the selected patches with position embeddings to retain position information, capable of capturing the global and local information of inter- and intra-patches. This method has been applied for the AD classification and the prediction of the transitional state moderate cognitive impairment (MCI) conversion with real datasets. The experimental evaluation shows that the proposed method can identify discriminative pathological locations effectively with a significant reduction on patch numbers used, providing better performance in terms of accuracy,

computing performance, and generalizability, in contrast to the state-of-the-art methods.

Index Terms—Deep learning, Feature extraction, Alzheimer's disease, Brain modeling, Structural MRI

I. INTRODUCTION

Alzheimer's disease (AD) is a degenerative brain illness and the most prevalent cause of dementia, accounting for 60% to 80% of cases [1]. Currently, there is no cure for AD. However, an accurate and timely AD diagnosis can give patients the best chance to prepare a treatment plan that may change the disease progression and reduce the symptom [2]. So far, brain atrophy [3], gray matter atrophy [4], and regional atrophy [5], are considered as the most critical neurodegeneration bio-markers. Structural magnetic resonance imaging (sMRI) as a non-invasive method measures brain morphometry, and is able to capture the subtle brain changes induced by the atrophic process, thanks to its high contrast for soft tissues and high spatial resolution [6]. It has been used in detecting AD and moderate cognitive impairment (MCI) with various computer vision methods [6]–[8]. The existing sMRI-based AD diagnostic methods usually partition the entire MR image into multiple regions for better feature extraction of local abnormal brain structural changes [9]–[13]. Depending on the partition scale, it can be broadly grouped into three categories: 1) Voxel-based; 2) Regions of interest (ROIs)-based and 3) Patch-based methods.

The voxel-based sMRI diagnostic methods take whole images as input and extract global voxel-wise features for AD diagnosis [14]–[16]. Features such as the probability maps of gray matter (GM) [14], white matter (WM) [17], and cerebrospinal fluid (CSF) [18] are widely used. However, there exist some limitations [19] including 1) Due to the high dimensionality of the feature extracted from the data, the number of data used for model training is relatively small, resulting in computationally intensive and over-fitting. 2) Ignoring area information of brain that has been shown to be important in the diagnosis of AD.

To alleviate the aforementioned problems, several existing works focused on some predetermined ROIs guided by prior

Xin Zhang, Liangxiu Han, Darren Dancey are with the Department of Computing, and Mathematics, Manchester Metropolitan University, Manchester M15GD, U.K (e-mail: x.zhang@mmu.ac.uk; l.han@mmu.ac.uk, d.dancey@mmu.ac.uk)

Lianghao Han is with the Department of Computer Science, Brunel University, Uxbridge UB8 3PH, U.K (e-mail: lianghao.han@brunel.ac.uk)

Haoming Chen is with the Department of Computer Science, University of Sheffield, Sheffield S1 4DP U.K (e-mail: hchen78@sheffield.ac.uk)

Daoqiang Zhang is with College of Computer Science and Technology, Nanjing University of Aeronautics and Astronautics, P.R.China (e-mail: dqzhang@nuaa.edu.cn)

Corresponding author*: L. Han (e-mail: l.han@mmu.ac.uk)

biological knowledge and extracted regional features for AD diagnosis [20]–[25]. However since these methods are based on empirical regions, they might neglect possible pathological locations in the whole brain [26]. The features extracted from the ROI may not capture the microscopic variation that is involved in the brain [27]. Additionally, segmenting ROIs based on expert knowledge is resource intensive.

To locate the subtle brain atrophy regions for the early diagnosis of AD and avoid fine-grained segmentation, patch-based methods, as a compromise between voxel-based and ROI-based methods, are proposed for the effective capture of small local structural changes in sMRI images. Unlike the other two types of methods, this type of methods segments an sMRI image into multiple small fixed-size regular 3D patches based on prior-knowledge/pre-defined anatomical landmarks [26], [28], [29] or statistics methods [30]. However, the pre-defined patch selection approach may miss some AD-related atrophy patches. Statistic analysis such as the T-test does not necessarily identify the correct regions linked with AD due to carry-over effects and lacks explainability [31]. In these approaches, the feature extraction and classification from the selected patches are often based on conventional machine learning methods such as Support Vector Machines (SVM) [32], and Linear programming boosting [33]. In [34]–[36], the authors used the handcrafted features, which may degrade the classification performance due to the heterogeneity between features and subsequent classification algorithms. Recently, deep learning methods based on convolutional neural networks (CNNs) for AD diagnosis directly learn feature representations from input patches without needing feature selection [26], [29], [30], [37], [38], making the whole process much more convenient and less prone to error and bias. However, in these methods, an image is firstly partitioned into patches and then each selected input patch is fed into the CNN independently. The local position information of each patch and the spatial relationship between patches are not included in the CNN computation. Few deep learning methods with the black-box nature of neural networks have specific output functions for pathological location positioning. As cerebral atrophy typically appears to be localised, only a few areas on sMRI scanning have significant structural changes highly correlated with the pathological characteristics, while the remaining areas give few useful distinguishing information. Hence, two remaining challenges in the patch-based methods are 1) how to accurately locate and select the patches; 2) how to capture both local and global features for improved explainable AD diagnosis. To address these challenges, this work proposes a novel patch-based neural network (sMRI-PatchNet) with explainable patch localisation and selection for Alzheimer’s disease diagnosis and discriminative atrophy using Structural MRI. Our contributions include:

- 1) An explainable patch localisation and selection for discriminative atrophy regions is proposed, in which the fewest number of AD-related patches with explainability are selected based on a novel fast recursive partition perturbation method for computing the SHapley Additive exPlanations (SHAP) contribution to a transfer learning

model for AD diagnosis on massive medical data. This significantly reduces computational complexity and enhances explainability.

- 2) A novel patch-based deep learning model (sMRI-PatchNet) is proposed for improving AD diagnosis performance, in which a learned position embedding is added to the patch presentation to retain the position and spatial relationship of patches. The sMRI-PatchNet has three main parts: Global spatial information (GSI) and Local patch information (LPI), are used to capture global feature between patches and local features within a patch efficiently, and a classifier for feature classification.
- 3) The proposed approach has been evaluated against real datasets with the corresponding visualization. From a clinical perspective, the visualization results of brain regions covered by selected patches show that the proposed method can effectively identify discriminative pathological locations. These new biomarkers can help clinicians in clinical diagnosis.

The remaining part of this paper is organized as follows: Section 2 presents the related work; Section 3 details the proposed method; Section 4 and 5 describe the experimental evaluation and results. Section 6 provides the discussion on the potential of clinical translation and the limitations of the proposed work; Section 7 concludes the work.

II. RELATED WORK

In this section, we review patch-based brain diagnosis methods using sMRI and explainable artificial intelligence methods.

A. Patch-based brain diagnosis methods in sMRI

Based on partitioning scales, the existing sMRI-based AD diagnostic methods can be broadly divided into three categories: 1) voxel-based, 2) regions of interest (ROIs) based, and 3) patch-based methods. The voxel-based methods are intuitive and straightforward in terms of the interpretation of results, aiming to identify disease-related microstructures from sMRIs of patients. The key point of this type of methods is to find suitable image features to estimate the probability of different tissue classes in a given voxel, such as gray matter (GM), white matter (WM), and cerebrospinal fluid (CSF) [39]. However, only analysing the features of isolated voxels would lead to the ignorance of high correlations between voxels. Another limitation of voxel-level methods is the overfitting problem because the voxel-level feature representations always have higher dimensionality compared with the number of image samples in model training. Several feature dimensionality reduction algorithms are used to solve this issue, e.g. a sparse coding method with a hierarchical tree-guided regularisation [40]. An alternative solution to feature extraction is to use 3D CNN. In [41], the authors have demonstrated that using 3D CNNs to extract features for AD classification can achieve better accuracy than traditional hand-crafted feature extraction approaches. In [13], the authors have designed a self-attention 3D CNN to improve the diagnosis performance by adding attention to global features. However, the main limitation

of 3D CNN methods is their extra-high computation costs caused by 3D convolution operations. In contrast, ROI-based approaches are based on the predefined regions identified from prior biological knowledge, such as the shrinkage of cerebral cortices, hippocampi and ventricles etc. [22], [24], [42]. These methods require a much lower feature dimensionality than the whole voxel-based methods. However, disease-related structural/functional changes occur in multiple brain regions. The ROI-based approach may neglect disease-related features or fail to capture small and subtle changes associated with brain diseases [27]. Additionally, segmenting ROIs based on experts knowledge is resource intensive, which remains a challenging task [29].

To address these limitations, the patch-based methods have been proposed, in which brain regions are split into several small fix-sized 3D patches. Regular patches eliminate the need for region segmentation in the dataset, and each patch is a region of interest. Since brain atrophy usually occurs locally, only a few of the regions in sMRI scans have noticeable structural changes, highly associated with pathological features. The existing works have been mainly focusing on two main challenges :1) how to select patches and combine the local patches to capture global information of the whole brain sMRI? 2) how to extract representative features and classify the patches into the right categories?

For the first challenge, empirical knowledge-based and statistical analysis-based methods have been used for the patch selection. On one hand, the empirical knowledge-based methods select the patches in the important regions based on prior knowledge. For example, Lian et al [26] adopted anatomical landmarks defined in the whole brain image as prior knowledge for generating selected patches. These anatomic landmarks were defined using a shape constraint regression forest model [27]. On the other hand, the statistical analysis-based selection methods use statistical algorithms to calculate the patch differences between Alzheimer's disease (AD) and Normal cohort (NC) patients. The patches with the highest variance are selected as the discriminative patches. In previous studies [29], [30], [40], [43], a T-test was used to find the difference between AD patients and NC group data for each patch. The patches with p-values smaller than 0.05 were selected. In the study [44], the authors used the weighted correlation coefficient [45] as the similarity measure to select discriminative patches. However, the statistical significance for voxels in each patch does not necessarily have a link with AD. Therefore, the explainable patch selection is still a challenging task.

For the second challenge, research efforts have been made on the feature extraction and classification of patched data. Liu et al. [43] first developed a patch-based AD diagnosis method with an independent feature extraction for each patch. The features were then integrated hierarchically at the classifier level. Inspired by Liu's method, Suk et al. [29] proposed a systematic method for a joint feature representation from the paired patches of sMRI images using a patch-based approach. Tong et al. [46] developed a multiple instance learning (MIL) model for AD classification and MCI conversion prediction using local intensity patches as features. Zhu et al. [30]

proposed a dual attention multi-instance deep learning network (DA-MIDL) for the early diagnosis of AD, in which a Patch-Nets with spatial attention blocks was used for extracting discriminative features of each patch. It has been proven that these patch-based methods can efficiently deal with the problem of high dimensional features and sensitivity to slight brain structure changes.

However, in the patch-based approaches described above, each selected patch is fed into the CNN independently. The local position information of each patch and the spatial relationship between patches are not included in the CNN computation. Few deep learning methods with the black-box nature of neural networks have specific output functions for pathological location positioning. Therefore, accurately identifying the discriminative patches while capturing both local and global features for improved explainable AD diagnosis is still a remaining challenge in patch-level methods.

B. Explainable methods

Recently, machine learning (ML) methods, including deep learning (DL), have been enormously successful in various fields [47]. However, they are still seen as a "black box" model due to their multilayer nonlinear structure. These models have been criticized for lack of transparency, and their predicted results are not traceable [48]. Interpreting and explaining a "black box" model is extremely important in real applications. A reasonable interpretation of an ML model can increase the user's trust and provide helpful information to improve the model. So far, there have been many general interpretation methods for ML/DL models, and have given birth to a new subfield, explainable artificial intelligence (XAI) [49]. Based on the algorithmic approaches used, the XAI methods in medical image analysis for visual explanation can be categorized into two types: backpropagation-based and perturbation-based methods [50]. The backpropagation-based methods focus on the back-propagation of gradients through the neural network to highlight pixel attributions [51], [52]. The saliency map is the first interpretation method that generates a visual explanation using the back-propagation on the convolutional network [52]. The guided back-propagation method is another gradient-based XAI method to improve the saliency map by restricting the back-propagation of values less than 0 [53]. Class Activation Mapping (CAM) is also a widely used XAI method. The CAM replaces the last fully connected layers with convolutional layers to keep the object positions. This operation help discover the spatial distribution of discriminative regions for the predicted category [54]. In the paper [13], the authors used the CAM method to explain the deep learning model's decision on AD diagnosis. However, the backpropagation-based methods are criticized for being inherently dependent on the model and data-generating process [55]. Ghorbani et al. [56] and Kindermans et al. [57] have shown that small perturbations or simple transformations to the input generated much more significant changes in the interpretations than the backpropagation-based methods did. The perturbation-based XAI methods focus on perturbing the input to assess the attribution of pixels in certain areas. The

feature set of the input is perturbed through occlusion, removing, masking, conditional sampling, and other techniques. Then, the forward pass of the perturbed input is used to generate the attribution representations without the need for backpropagating gradients [58], [59]. The Local Interpretable Model-Agnostic Explanations (LIME) is one of the most widely used perturbation-based XAI methods because it can explain any classifier in an interpretable and faithful manner [59]. To generate a representation that explains the model's decision, LIME tries to find the importance of contiguous super-pixels in an input image towards the output class. Shapley additive explanations (SHAP) is a similar method that uses the classical Shapley values from game theory to show the importance to the models [60], [61]. However, the perturbation-based XAI methods have the challenge of combinatorial complexity explosion. This happens when one attempts to go through all elements of the input and all their possible combinations to observe how each of them would affect the output [62]. The possible combinations of data perturbations increase dramatically when dealing with 3D images, causing a significant increase in computational costs. To avoid the combinatorial explosion, a fast perturbation method is proposed in this paper.

III. THE PROPOSED METHOD

This study aims to propose a novel patch-based convolutional network (sMRI-PatchNet) with an explainable patch selection for AD diagnosis with sMRI images. It involves two-level classifications: Alzheimer's disease (AD) vs. Normal cohort (NC), and progressive MCI (pMCI) vs. Stable MCI (sMCI).

The schematic diagram of our framework is shown in Fig. 1, which consists of two major units: Explainable Patch Localisation and Selection (EPLS) for patch selection and sMRI-PatchNet for feature extraction and classification. The rationale behind this architecture includes:

- 1) Unlike traditional statistical or prior knowledge-based methods, we have proposed an explainable patch localisation and selection method. It can accurately identify the fewest number of AD-related patches based on a novel fast recursive partition perturbation method for computing the SHapley Additive exPlanations (SHAP) contribution to a transfer learning model for AD diagnosis on massive medical data. This significantly reduces computational complexity and enhances explainability.
- 2) A novel patch-based deep learning network (sMRI-PatchNet) is proposed for feature extraction and classification. The selected patches are flattened into vectors using a linear projection. A learned position embedding is added to the patch presentation to retain their location and spatial information. Two CNN blocks including global spatial information (GSI) and local patch information (LPI) are proposed to capture the global features between patches and local features within a patch. A classifier consisting of average pooling followed by a fully connected layer is connected to predict output classes.

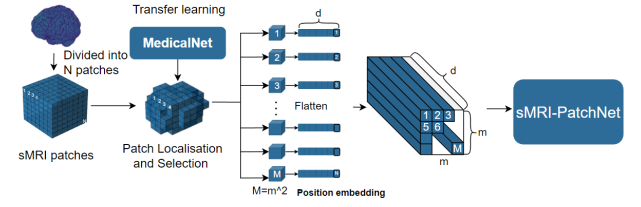


Fig. 1. The flowchart of the proposed method

A. Explainable Patch Localisation and Selection (EPLS)

The unit of explainable patch localisation and selection (EPLS) aims to identify and select the most discriminative patches by evaluating their importance to the AD diagnosis (classification). It was implemented through transfer learning using MedicalNet [63] pretrained on 23 publicly available large medical image data, and fine-tuned with an sMRI dataset. The classification accuracy of MedicalNet can reach 0.909. As shown in Fig. 2, in this unit, each sMRI image is uniformly partitioned into 3D cubic patches with a fixed size, without overlapping. Based on our experiments and the previous work [26], the size of $25 \times 25 \times 25$ is selected in this study. These patches are fed into the MedicalNet for evaluating their importance to AD diagnosis. A fast explainable recursive partition perturbation approach for assessing the patch importance based on the value of the SHAP coefficient has been designed. To explain the model's decision, we perturb the sMRI data by filling value of 0 on specific patch and observing how the model output changes to the perturbations. Then, the SHAP coefficient is calculated to measure the contribution of each location of the sMRI input to the model output. This is aligned with human intuition and can effectually discriminate among model output classes [61]. We average the contribution of each location for all sMRI images identified as AD, and the high contribution locations are selected as input to the AD diagnosis model.

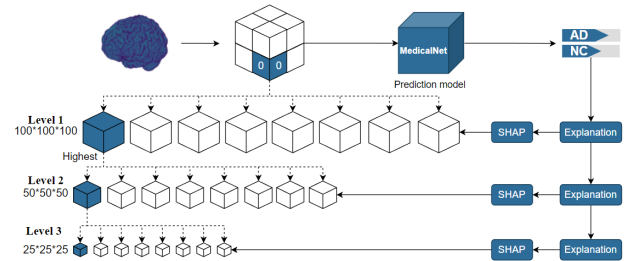


Fig. 2. The flowchart of the fast recursive partition XAI method

1) Fast recursive partition perturbation method: In this work, each sMRI image is divided into n 3D cubic patches ($n=598$ when the patch size is $25 \times 25 \times 25$ on a standard sMRI image). The computational complexity of the model explanation on each image will be 2^n by using the conventional permutation method to perturb the data. This will take an unacceptable amount of time to work through all the sMRI data.

To reduce the computational complexity and costs without compromising the performance, this work introduces a fast recursive partition perturbation method to perturb the image

hierarchically. Unlike the conventional permutation methods which ignore the link between patches, our proposed method calculates the importance of each patch by iteratively partitioning the data. The algorithm is shown in Fig. 3. Specifically, to avoid predefining regions of interest, we partition an image, X , into disjointed regular patches ($X_{1,0}, X_{1,1}, X_{1,2} \dots X_{1,n}$), called level 1, the size of each patch is $100 \times 100 \times 100$, and n is the number of patches ($n = 8$ is chosen at Level 1 for 3D images). After computing the SHAP coefficients of all patches at Level 1, ($S_{1,0}, S_{1,1}, S_{1,2} \dots S_{1,n}$), we further partition each patch into 8 smaller sub-patches in a hierarchical manner up to Level 3, based on its SHAP value. If the calculated SHAP coefficient for a patch is greater than a pre-defined threshold (τ), then there is no further partition to the next level; or else, if $S_{1,i} < \tau$, we partition this patch to the next level; and recursive this manner up to Level 3. The patch sizes are $50 \times 50 \times 50$ at Level 2 and $25 \times 25 \times 25$ at Level 3. After the recursion, all the patches along with their SHAP coefficient values are returned.

This partitioning method matches the data structure of the image and significantly reduces the computational complexity.

Algorithm 1 Fast recursive partition Shap algorithm (R-Shap)

Input:
 X : sMRI data;
 τ : Threshold $\tau \geq 0$;
 f : The prior knowledge model;
1: procedure $R - \text{Shap}(X_l, f, \tau)$ # R-Shap algorithm for level l ;
2: $X \rightarrow X_1 = (X_{1,0}, X_{1,1}, X_{1,2} \dots X_{1,n})$ # Partition the input X into disjoint regular patches X_l ;
3: $(X_1, f) \rightarrow g_1$ # Set a n -person cooperative game;
4: $s_{1,0}, s_{1,1}, s_{1,2} \dots s_{1,n} \leftarrow \text{Shap}(g_1)$ # Calculate the Shap value for each patch;
5: **for** s **in** s_1 **do**
6: **if** $s < \tau$ **then**
7: Return s
8: **else**
9: Return $R - \text{Shap}(X_{l+1}, f, \tau)$ # Calculate the shap value for level $l+1$;
10: **end if**
11: **end for**

Fig. 3. 3.1.1. Fast recursive partition perturbation method

2) SHAP coefficient estimation method: The SHAP coefficient [60] is used to calculate the contribution of each patch towards the output of AD classification) and can be defined as:

$$S_i(f) = \sum_{C \subseteq [n] \setminus \{i\}} \frac{|C|!(n - |C| - 1)!}{n!} [f(X_{C \cup \{i\}}) - f(X_C)] \quad (1)$$

Where C is a subset of n patches used in the model, X is the vector of all patch features and n is the number of patches in the input. $f(X_{C \cup \{i\}})$ is the predicted probability of AD with the i th patch included while $f(X_C)$ is the probability value without the i th patch in the input. $S_i(f)$ represents the averaged marginalized contribution of i th patch over all possible subsets of n . The computation complexity is exponential in the dimension of the input features ($O(2^n)$).

B. sMRI-PatchNet

The second major unit is a patch-based deep learning convolutional network for feature extraction and classification, named sMRI-PatchNet, as shown in Fig. 4. After the patch

selection, these selected patches are flattened into vectors ($x_p \in \mathbb{R}^{M \times (P^3)}$) and mapped to d dimensions (the size of vectors) using a linear projection. Where P is the size of the patch, and M is the number of selected patches. To retain the positional information, a learned 1D position embedding [64] is added to the patch vectors.

$$X = [x_p^1 E; x_p^2 E; \dots; x_p^M E] + E_{\text{pos}}, \quad E \in \mathbb{R}^{(P^3) \times d}, E_{\text{pos}} \in \mathbb{R}^{(P^3) \times d} \quad (2)$$

We then group patch vectors in sequence to a new array ($X \in \mathbb{R}^{(d+1) \times (m \times m)}$), where $m \times m = M$ is the number of patches, d is the size of the array's Z-axis which denotes the dimension of each flattened patch. The Z-axis (d) represents the information inside each patch. The xy-axis ($m \times m$) represents the spatial information between the different small patches. The sMRI-PatchNet consists of global spatial information (GSI), local patch information (LPI), and a classifier. GSI is used to capture global information between the patches from the XY-axis and the LPI is used to capture the local features within a patch from Z-axis (d). The classifier consists of average pooling and a fully connected layer that classifies features into the correct class.

1) Global spatial information (GSI): The GSI is proposed to capture the global spatial information of patches. In the first part, the 3D patches are flattened into vectors and then converted to a 2D array ($X \in \mathbb{R}^{d \times (m \times m)}$), which can reduce the computational consumption caused by 3D convolution. Then a spatial-wise 2D convolution with a large kernel size of $m \times m$ is used to operate on $X \in \mathbb{R}^{d \times (m \times m)}$ to extract the global spatial information. The kernel size $m \times m$ allows the receptive field of convolution to cover the entire area. Then, the conventional activation (σ , Rectified Linear Unit(ReLU) [65]) and BatchNorm (BN [66]) are used following the GSI module to accelerate the model training. A residual connection [67] is introduced before and after the GSI to avoid the gradient vanishing problem when the depth of the model is increased.

$$X'_l = \text{BN}(\text{SpatialwiseConv}(X_{l-1})) + X_{l-1} \quad (3)$$

2) Local patch information (LPI): The LPI is proposed to capture the internal information of each patch. Note that the voxel values of each patch are flattened on the Z-axis in the input array with dimension d . Therefore, a pointwise 2D convolution with kernel size 1×1 , regarded as a multilayer perceptron (MLP), is executed on the channel axes. The activation and Batchnorm are also followed after the LPI module.

$$Z_{l+1} = \text{BN}(\sigma(\text{PointwiseConv}(X'_l))) \quad (4)$$

IV. EXPERIMENTAL EVALUATION

A. Dataset description and preprocessing

This study used the ADNI dataset, which was obtained from the public Alzheimer's Disease Neuroimaging Initiative (ADNI) database (<http://adni.loni.usc.edu>). In the ADNI

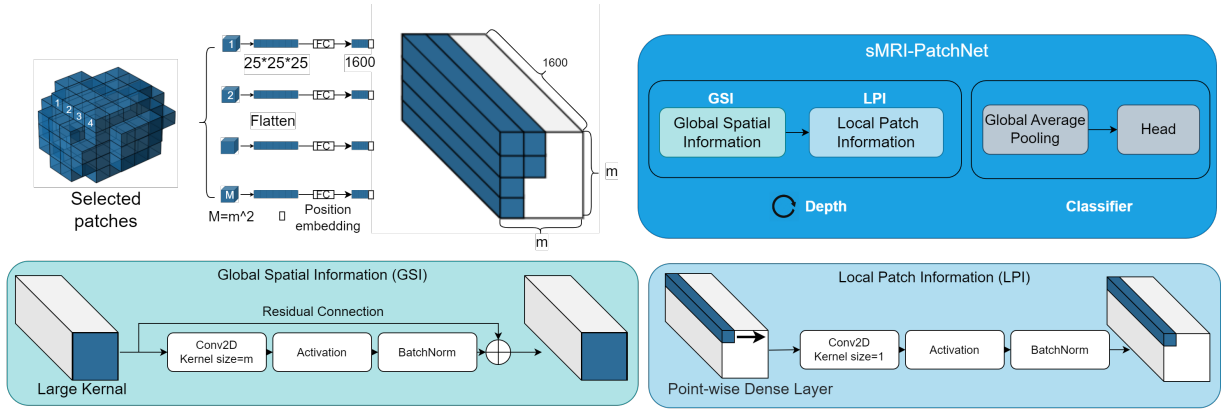


Fig. 4. The architecture of the sMRI-PatchNet Model

dataset, a total of 1193 1.5T/3T T1-weighted structural magnetic resonance imaging (sMRI) scans are taken from the baseline/screening visits (i.e. first examination) of subjects in the three ADNI phases (ADNI-1, ADNI-2 and ADNI-3). These participants can be classified into three groups: AD (Alzheimer's disease), MCI (mild cognitive impairment) and NC (normal controls) according to standard clinical criterias. For the prediction of MCI conversion, MCI subjects are further categorised into two groups: pMCI (progressive MCI subjects who convert to AD within 36 months of the baseline visit) and sMCI (stable MCI subjects who are consistently diagnosed with MCI). The study's ADNI dataset contained 389 AD, 172 pMCI, 232 sMCI and 400 NC subjects. The demographic details of this dataset are described in Table. I.

TABLE I

DEMOGRAPHIC DETAILS OF THE STUDIED SUBJECTS INCLUDING DATASET, GROUP TYPE, GENDER, AGE, MINI-MENTAL STATE EXAMINATION (MMSE) AND CLINICAL DEMENTIA RATING (CDR).

Dataset	Group	Gender (Male/Female)	Age (Mean±Std)	Edu (Mean±Std)	MMSE (Mean±Std)
ADNI-1	AD	200 (103 / 97)	75.62 ± 7.70	14.68 ± 3.20	23.29 ± 2.04
	pMCI	172 (106 / 66)	76.34 ± 7.15	15.76 ± 2.84	26.61 ± 1.70
	sMCI	232 (154 / 78)	76.47 ± 7.82	15.58 ± 3.17	27.31 ± 1.79
	NC	231 (119 / 112)	75.99 ± 5.00	16.06 ± 2.84	29.12 ± 0.99
ADNI-2/3	AD	153 (85 / 68)	74.95 ± 7.80	15.88 ± 2.66	23.03 ± 2.14
	NC	419 (170 / 249)	74.84 ± 6.60	16.63 ± 2.48	29.09 ± 1.19

The original structural MRI data from the ADNI database are pre-processed for subsequent feature learning and classification. As the original dataset is in Neuroimaging Informatics Technology Initiative (NIfTI) format, the preprocess is needed for spatial distortion correction caused by gradient nonlinearity and B1 field inhomogeneity. This is a standard pipeline process including anterior commissure (AC)-posterior commissure (PC) correction, intensity correction [68], and skull stripping [69]. We have used MIPAV (Medical Image Processing, Analysis, and Visualisation) application to implement AC-PC correction and use FSL (FMRIB Software Library v6.0) for skull stripping. A linear registration strategy (flirt instruction in FSL) is also executed to align every sMRI linearly with the Colin27 template [70] to delete global linear differences (including global translation, scale, and rotation differences), and also to re-sample all sMRIs to have the identical spatial resolution. After the preprocessing, all sMRI

images have the same size, containing $181 \times 217 \times 181$ voxels.

B. Evaluation metrics

We have evaluated two binary classification tasks: AD classification (i.e., AD vs. NC) and MCI conversion prediction (i.e., pMCI vs. sMCI). The classification performance is evaluated based on four commonly used standard metrics, including classification accuracy (ACC), sensitivity (SEN), specificity (SPE), and Area under the curve (AUC). These metrics are defined as:

$$ACC = \frac{TP + TN}{TP + TN + FP + FN} \quad (5)$$

$$SEN = \frac{TP}{TP + FN} \quad (6)$$

$$SPE = \frac{TN}{TN + FP} \quad (7)$$

Where $TP = TruePositive$, $TN = TrueNegative$, $FP = FalsePositive$ and $FN = FalseNegative$. The AUC is calculated based on all possible SEN and 1-SPE obtained by changing the thresholds performed on the classification scores yielded by the trained networks.

C. Experimental evaluation

To evaluate the performance of our proposed model, we have conducted three types of experiments: 1) Diagnostic performance evaluation. 2) Generalisability evaluation and 3) Impact of discriminative patch location selection on model performance.

1) *Experiment One: Diagnostic performance evaluation* : In this experiment, we evaluate the diagnostic performance of our proposed model. The detailed configuration of the proposed PatchNet is shown in Table. II. The patch size is $25 \times 25 \times 25$, and top 36 patches with the highest SHAP value are selected. These configurations are the best combinations obtained in our experiments. The model has 16 layers (D). The dimension of the flattened patch is 1600.

The proposed model is compared with several commonly used automatic AD diagnosis methods, including

TABLE II
THE MODEL CONFIGURATION

Model	sMRI-PatchNet
Patch size	25
Patch number	36
Heads	Na
Depth (D)	12
Dimension	1600
Param (M)	34.53

1) Three traditional machine learning (ML) based methods representing a typical example of the three types of existing computer-aided diagnostic methods for AD, respectively including:

a) A voxel-based method (VBM) from Ashburner et al [71]. In VBM, each sMRI is processed by the spatial normalization to a standard stereotactic brain space (i.e., Colin27 template) and the local gray matter density is measured as the voxel-level feature.

b) A region-based method (RBM) by Zhang et al, [72]. The RBM uses the prior knowledge identified regions of the sMRI image as the input. After a deformable registration [73], an entire brain sMRI image is segmented into 93 areas according to the template with 93 manually labeled ROIs [74], as described in [72]. The grey matter volume in each ROI is then calculated as a region-level feature, which is normalized by the total intracranial volume;

c) A patch-based method (PBM) from Zhang et al. [40]. The PBM uses selected patches as the input. The patch location selection method proposed in their study is used to evaluate the contribution of each patch to AD. The top 40 patches are selected, and a patch pool is operated on selected patches from tissue density maps to generate input vectors. The Light Gradient Boosting Machine (LightGBM) machine learning classifier is selected for feature classification. It has state-of-the-art accuracy, lower memory usage, and higher efficiency that can handle large-scale data [75]. The detailed parameters for the LightGBM classifier are shown in Table. III.

2) One deep learning model based on transfer learning: The MedicalNet (Med3D) [63]. It is also the trained model that we used for the explainable discriminative location selection. The Med3D adopts the ResNet family (ResNet 10, ResNet 18) architecture as the backbone [67]. To enable the Med3D to train with 3D medical data, all 2D convolution kernels are replaced with their 3D versions. To avoid overfitting when trained on the limited volume of training data, Med3D collected the dataset from several medical challenges to build a large dataset and provided a pre-trained model for other downstream tasks. In this work, we use this pre-trained model and fine-tune it with sMRI data for our AD diagnosis tasks.

3) Two typical patch-based deep learning methods, HFCN [26] and DA-MIDL [30]. Both of these methods used the statistical method for patch selection and proposed novel CNN models for patch feature extraction and classification. The HFCN model is implemented by multi-layer convolutional structures. It contains three-level networks consisting of patch-

level, region-level, and subject-level sub-networks. Multi-scale feature representations are jointly learned and fused for the construction of hierarchical classifiers. The features from different levels are spatially combined to feed into the classifier. The DA-MIDL model consists of three primary components: a) Patch-Nets with spatial attention blocks for extracting features within each patch; b) an attention multi-instance learning (MIL) pooling operation for balancing the relative contribution of each patch, and c) an attention-aware global classifier for further learning the features and making the AD-related classification decisions.

TABLE III
THE LIGHTGBM CLASSIFIER TRAINING PARAMETERS

Parameters	Description	Value
Boosting_type	Method of boosting	Gradient-boosted decision trees (gbdt)
Num_leaves	Max number of leaves in one tree	31
Max_depth	Limit the max depth For tree model, -1 means no limit	-1
Num_iterations	Number of boosting iterations	100
Learning_rate	The shrinkage rate for model train	0.05

In this test, we train our model using the ADNI-1 dataset and perform 10 times of five-fold cross-validation. The dataset is randomly split into five groups where four groups (80% of the dataset) are used for training, and the rest are used for testing. The experimental results for classification performance are the average of the accuracies and its standard deviation on the testing set across all folds. This allowed a more appropriate model analysis and made it possible to avoid overfitting problems. To optimize model parameters, Adam [76], a stochastic optimization algorithm with a batch size of 8 samples, has been used in training the proposed network. We first set the initial learning rate (LR) as 1×10^{-4} . The LR is decreased to 1×10^{-6} with increased iterations. CrossEntropy has been selected as the loss function for this task [77]. The experiments are implemented based on PyTorch and executed on a server with an Intel(R) Xeon(R) CPU E5-2650, NVIDIA 2080TI, and 64 GB memory.

2) *Experiment Two: Generalisability Evaluation* : In this experiment, the generalisability and repeatability of the proposed PatchNet model are evaluated. We train the model based on the whole ADNI-1 dataset and test it on two independent datasets (ADNI-2 and ADNI-3). Due to a lack of pMCI and sMCI samples from ADNI-2 and ADNI-3, we only evaluate the model performance on the AD vs. NC classification task. The four automatic diagnosis methods described in the previous section are used for comparison.

3) *Experiment Three: The impact of discriminative patch selection on model performance*: In this experiment, we evaluate the influence of patch selections on the classification performance of our proposed classification model, based on two different patch selection approaches, our SHAP-based method, and the traditional statistic method. We investigate the effect of the patch number on classification performance and the performance of two different patch selection methods on identifying the locations of patches in the brain. Considering that the patch choice is based on its contribution to AD, we use the AD vs. NC classification task for evaluation. In our SHAP-based patch selection approach, the top 16, 36, and 64 patches with the highest SHAP value are selected, respectively. The number of selected patches has to be squareable to match

the PatchNet requirement (that is, it can be converted to an $m \times m$ array). The traditional statistical analysis-based patch selection method used in [29], [30], [40], [43] is selected for comparison. This method assumes that the patch locations with the most significant differences between the AD and NC groups are more likely to be the brain regions with abnormal atrophy. Thus, the t-test [78] is applied to two groups of patch-level features at one patch location from the same amount of AD patients and normal controls in the training set, respectively. The p-value for each patch location is used to sort the informativeness in all patches. The patches with lower p-values are selected. Here we orderly select the number from 20, 40, 60, 120, 200 in the PatchNet and record the corresponding results. Identifying morphological changes in the brain can help the clinical diagnosis of AD [5], [79], [80]. To investigate the performance of the two patch selection methods on identifying the brain regions associated with AD, we quantitatively visualize the patch locations predicted as AD and the regions where they are located in the brain. Accurately identifying these regions can provide valuable information for clinical diagnosis.

V. RESULTS

A. Results of Diagnostic Performance Evaluation

The results of AD vs. NC classification and MCI conversion prediction achieved by our sMRI-PatchNet model and the competing methods on the ADNI-1 dataset are shown in Table. IV. The proposed sMRI-PatchNet method achieves the best accuracy (0.920 and 0.819) in the two classification tasks, which are statistically significant. Of the three machine learning-based baseline methods, the PBM outperforms the RBM and VBM methods, indicating that patch-level feature representations could offer better discriminative information regarding the subtle brain changes for brain disease diagnosis.

Moreover, as shown in Table. IV, the Med3D-18, which uses the whole image as input, surpasses the three traditional machine learning-based methods (WBM, RBM, and PBM) with different input representations by significant margins in both tasks. It demonstrates that with the transfer learning from the massive medical dataset training [63], Med3D can effectively extract useful high-level features from the entire sMRI image for the classification task. In addition, the deep learning-based methods learn high-level features from data in an incremental manner with a massive number of parameters and non-linear calculations, thus allowing better performance than traditional machine learning models.

B. Results of Generalizability Evaluation

Table. V shows the AD classification results of our method and the competing methods evaluated on the independent ADNI2 & 3 datasets. Our proposed sMRI-PatchNet generally outperforms the other five competing methods. the sMRI-PatchNet obtains the highest accuracy (0.891) in the AD vs. NC classification, outperforming VBM (0.806), RBM (0.789), PBM (0.825), Med3D-18 (0.874), HFCN (0.851) and DA-MIDL(0.868). These results indicate that the sMRI-PatchNet can provide robust performance across different datasets.

In general, the performance of a model is expected to decrease when evaluating on the independent dataset. The accuracy and AUC of our proposed model slightly decrease by 2% and 4%, respectively. These results indicate the good generalization capability of our method for AD diagnosis. The accuracy of machine learning-based methods, such as VBM, RBM, and PBM, only drops by around 1%. This may be due to the fact that the ML-based methods have fewer parameters, allowing the model to avoid overfitting.

C. The Impact of Discriminative Patch Location Selection on Model Performance

Fig. 5 shows the distributions of discriminative patches selected by the statistical analysis method and the proposed explainable SHAP-based method. The discriminative patch locations determined by the SHAP-based method focus more on the central part of the sMRI image, while the results from the statistical analysis method are discrete and distributed in various regions.

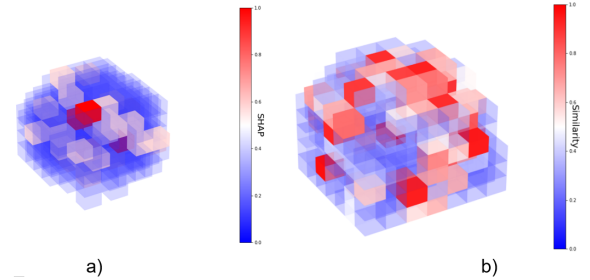


Fig. 5. The discriminative patch location distribution determined by: (a) the proposed explainable SHAP based method and (b) the statistic analysis method.

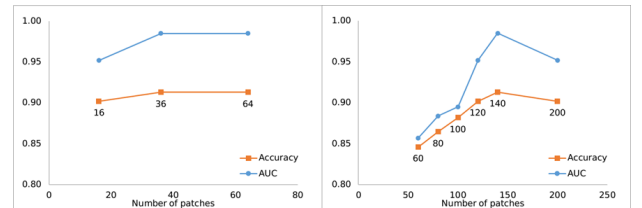


Fig. 6. Results of Accuracy and AUC in AD classification obtained by: (a) our proposed explainable SHAP-based method and (b) the statistic analysis method with different selected numbers of input image patches.

Fig. 6 shows the changes in the classification performance of our sMRI-PatchNet model with the increasing number of input image patches selected by the two methods, in terms of accuracy and AUC. It can be observed that PatchNet achieves satisfactory accuracy and AUC using the input patches selected by our proposed patch selection approach, even though the number of selected patches (n) is only 16. In contrast, the classification accuracy of PatchNet with the input patches selected by the statistic analysis method is only 0.846, after selecting a larger number (60) of input patches. Only under the circumstance of increasing the number of patches selected by the statistic method from 60 to 140, both the accuracy and AUC are significantly improved. This implies that the locations

TABLE IV
RESULTS FOR AD CLASSIFICATION (I.E., AD VS. NC) AND MCI CONVERSION PREDICTION (I.E., PMCI VS. SMCI)

Model	AD vs. NC classification				pMCI vs. sMCI classification			
	ACC	SEN	SPE	AUC	ACC	SEN	SPE	AUC
VBM [71]	0.815±0.043	0.755±0.05	0.873±0.036	0.884±0.037	0.682±0.054	0.629±0.08	0.714±0.06	0.706±0.053
RBM [72]	0.808±0.107	0.717±0.103	0.883±0.106	0.849±0.072	0.669±0.084	0.573±0.094	0.741±0.073	0.696±0.034
PBM [40]	0.838±0.089	0.726±0.124	0.871±0.05	0.847±0.028	0.682±0.071	0.4±0.096	0.73±0.071	0.637±0.048
Med3D-18 [63]	0.909±0.149	0.896±0.142	0.924±0.151	0.952±0.085	0.806±0.047	0.773±0.054	0.833±0.055	0.817±0.033
HFCN [26]	0.882±0.047	0.89±0.054	0.883±0.055	0.929±0.033	0.807±0.046	0.806±0.049	0.798±0.036	0.794±0.036
DA-MIDL [30]	0.904±0.079	0.887±0.092	0.903±0.075	0.922±0.034	0.809±0.092	0.771±0.101	0.826±0.097	0.851±0.047
Our Method	0.920±0.088	0.920±0.119	0.919±0.052	0.967±0.023	0.819±0.044	0.818±0.055	0.816±0.056	0.857±0.029

TABLE V
RESULTS OF AD CLASSIFICATION ON THE INDEPENDENT ADNI2 AND 3 DATASETS

Model	AD vs. NC classification			
	ACC	SEN	SPE	AUC
VBM	0.806±0.046	0.578±0.049	0.866±0.036	0.816±0.036
RBM	0.789±0.102	0.522±0.103	0.865±0.102	0.795±0.076
PBM	0.825±0.088	0.775±0.119	0.866±0.052	0.884±0.023
Med3D-18	0.874±0.147	0.795±0.141	0.915±0.148	0.906±0.089
HFCN	0.851±0.012	0.749±0.014	0.855±0.009	0.865±0.026
DA-MIDL	0.868±0.034	0.772±0.092	0.893±0.101	0.901±0.097
Our method	0.891±0.019	0.791±0.068	0.882±0.046	0.925±0.023

determined by the statistical methods are not necessarily correct, and a smaller number of patches are insufficient to yield satisfactory results. In our implementations, $n = 36$ is chosen to make a compromise between the computational complexity, the memory cost of training, and including a large enough number of potentially valuable locations.

VI. DISCUSSIONS

In this section, we first analyse the influence of the number and size of patch selection on the performance of the proposed model and its potential for clinical translation. Then, we compare our proposed method with previous studies on AD-related brain disease diagnosis.

A. Influence of Number and Size of Patches

As a patch-based method, the size and number of patches are important parameters. We discuss the influence of the number and size of patches on the performance of the proposed model. Fig. 6 a) shows the AD classification results achieved by the proposed model respectively with a range from 16 to 64. We can observe that both ACC and AUC are stable and better in the range of 16 to 64. The best performance is achieved when n increases to 36. This implies that small numbers of patches (e.g., $n=16$) may not include adequate patches related to AD classification. While, large numbers of patches (e.g., $N=64$) will increase the number of patches with useless information for AD classification.

In this paper, we select a patch size of $25 \times 25 \times 25$, the same as used [26], [30]. We evaluate the AD classification performance with different patch sizes. Fig. 7 shows the AD classification performance with different patch sizes in a range of $15 \times 15 \times 15$ to $35 \times 35 \times 35$. The result shows the proposed model achieve a stable performance for all selected patches, and indicating that the model is not sensitive to the size of input patches within this range. The accuracy of the proposed

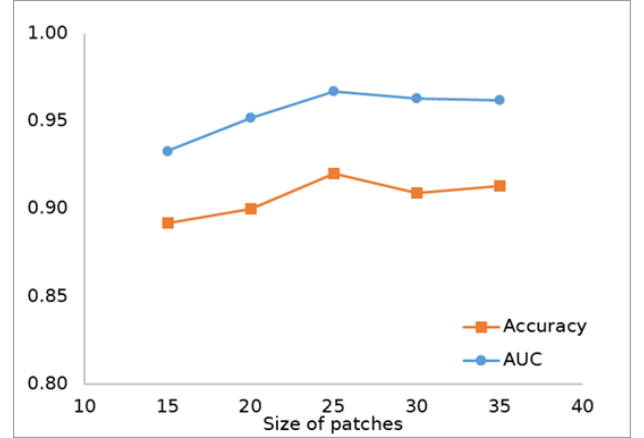


Fig. 7. AD classification performance of the proposed model with the input patches of different sizes ($15 \times 15 \times 15$ to $35 \times 35 \times 35$) on the ADNI test set.

model is greater than 0.9 for all selected patch sizes, except $15 \times 15 \times 15$. This implies that a relatively large patch size is required in order to capture sufficient details of feature changes by brain atrophy.

B. Discriminative Pathological Locations and the Potential of Clinical Translation

In Fig. 8, we visualize the locations of selected patches for AD diagnosis and their corresponding brain regions in the automated anatomical atlas (AAL 3V1) [81]. Nearly half of the suggested discriminative locations by the statistic method are in the Posterior fossa, and the rest are in the cerebrum.

However, the discriminative locations suggested by the proposed method cover 47 of 170 brain structures. Table. VI lists 31 brain regions to which the patches suggested by our SHAP-based approach correspond in the brain atlas AAL 3V. They include Frontal Lobe, Temporal Lobe, Posterior Fossa, Insula and Cingulate Gyri, Occipital Lobe, Parietal Lobe, Central Structures, etc. These regions, such as the Precentral gyrus, Superior frontal gyrus, Middle frontal gyrus, Inferior frontal gyrus [82], Supplementary motor area [83], Olfactory cortex [84], Hippocampus, Parahippocampal gyrus, Amygdala [85], Insula [86], Lingual gyrus [87], Precuneus [88], Caudate nucleus [89], etc. are reported to be associated with AD. Specifically, the hippocampus is strongly linked to long-term memory. The impact of AD-related brain shrinkage on the hippocampus has been scientifically validated [24]. The amygdala is considered to influence emotional functioning as

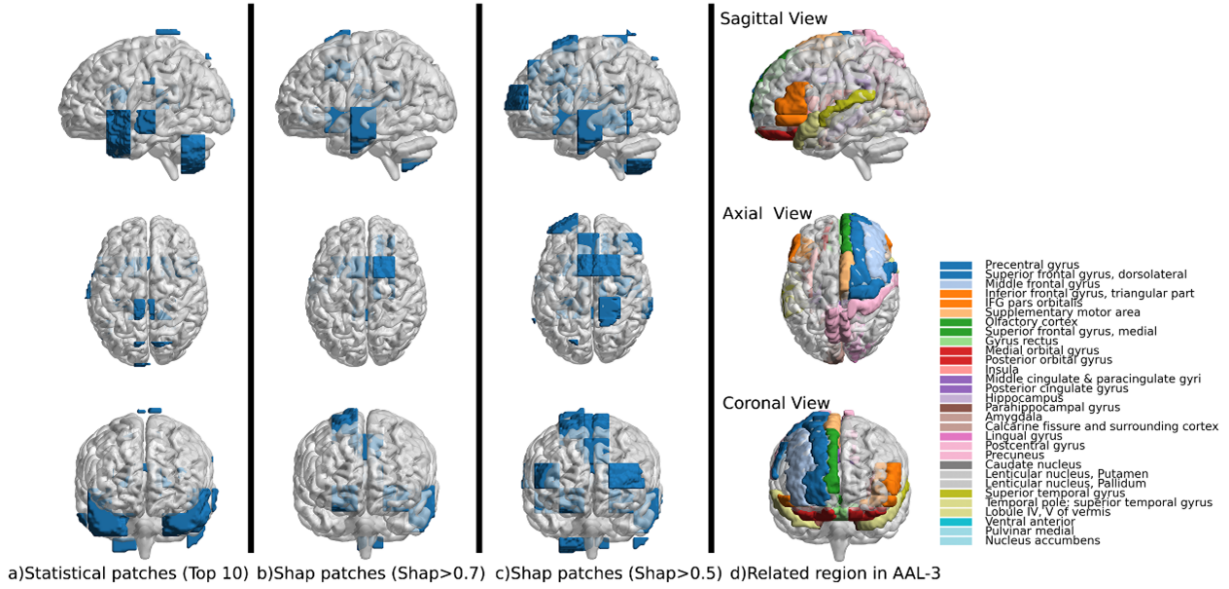


Fig. 8. Discriminative AD-associated locations automatically identified by our proposed explainable SHAP-based method and the statistic analysis method. The first column shows the top 10 informative patch locations suggested by the statistical analysis. The second and third columns show the informative patch locations suggested by the proposed SHAP-based method with thresholds 0.7 and 0.5, respectively. The rightmost column shows the marked brain regions where the suggested patches are gathered by the proposed method.

well as learning and memory management [90]. The thalamus is linked to cognition and information processing speed [91], which are also relevant to AD. These pieces of evidence imply the feasibility of our proposed method for identifying AD-associated areas and can inform clinicians on AD diagnosis.

TABLE VI

A LIST OF BRAIN REGIONS THAT THE SUGGESTED PATCHES FROM OUR METHOD COVER IN THE AUTOMATED ANATOMICAL ATLAS (AAL 3V1) [81].

Description	Code	Description	Code
Frontal Lobe		Insula and Cingulate Gyri	
Precentral gyrus	2	Insula	33,34
Superior frontal gyrus, dorsolateral	4	Middle cingulate & paracingulate gyri	38
Middle frontal gyrus	6	Posterior cingulate gyrus	39,40
Inferior frontal gyrus, triangular part	9	Occipital Lobe	
IFG pars orbitalis	11,12	Calcarine fissure and surrounding cortex	47
Supplementary motor area	16	Lingual gyrus	52
Olfactory cortex	17,18	Parietal Lobe	
Superior frontal gyrus, medial	20	Postcentral gyrus	62
Gyrus rectus	23,24	Precuneus	71,72
Medial orbital gyrus	25,26	Central Structures	
Posterior orbital gyrus	29,30	Caudate nucleus	75,76
Temporal Lobe		Lenticular nucleus, Putamen	77,78
Hippocampus	41	Lenticular nucleus, Pallidum	79,80
Parahippocampal gyrus	43,44	Pallidum (PAL)	81,82
Amygdala	45,46	Ventral anterior	126
Superior temporal gyrus	85	Pulvinar medial	145,146
Temporal pole: superior temporal gyrus	87,88	Nucleus accumbens	158
Posterior Fossa			
Lobe IV, V of vermis	115		

C. Comparison with Previous Works

For a broad comparison between our method and related studies on the performance of AD diagnosis, in Table 8 we list the results of several state-of-the-art models reported in the literature for AD classification and MCI conversion prediction tasks using structural MRI data from the ADNI database, including two voxel-level methods [13], [92], two ROI-level methods [93], [94] and four patch-level methods [26], [30], [43], [46]. The following observations can be noted in Table 8. 1) Our method has achieved a competitive performance in both

AD-related classification tasks. 2) Compared with traditional machine learning-based methods such as SVM [46], [92], LDA [94], and KNN [93], the deep learning-based methods have better performance, particularly for more difficult MCI conversion tasks. The possible reason is that deep learning methods have more parameters and can therefore deal with the spatial features and correlation of the 3D data better than machine learning methods. Compared to the other two deep learning patch-based methods, HFCN and DA-MIDL, the proposed method achieves better accuracy. As we mentioned in the Introduction section, the 3D convolution operation brings increased parameters and around six times the computational complexity (3x3 kernel size) than the 2D convolution operation. Table 6 shows the computational complexity and the number of parameters of the four deep learning-based methods. The Med3D with 10 layers, HFCN, DA-MIDL, and sMRI-PatchNet have a similar number of parameters (around 35 Million). The Med3D with 18 layers has the highest number of parameters (63.53 Million). However, in terms of computational complexity, the Med3D, HFCN and DA-MIDL are all use 3D convolution operation. Their computational complexities are 169.55 GMac and 240.73 GMac and 220.63 GMac, respectively. Our proposed sMRI-PatchNet uses 2D convolution and has the minimal computational complexity (2.21GMac). (3) Unlike ROI-based methods relying on empirically predetermined ROIs, the proposed sMRI-PatchNet automatically extracts important areas from multiple patches distributed in the whole brain. This is much more difficult. However, our method still obtains good performance, implying the effectiveness of our model for identifying the location of pathology.

TABLE VII

REFERENTIAL COMPARISON ON SMRI-BASED STUDIES FOR AD CLASSIFICATION AND MCI CONVERSION PREDICTION

References	Feature	Method	Subject	AD vs. NC classification		pMCI vs. sMCI classification	
[92]	Voxel-based	SVM	137AD+134sMCI+76pMCI+162NC	0.89	0.81	0.95	0.7
[13]		3D-CNN	353AD+232sMCI+172pMCI+591NC	0.91	0.91	0.92	0.82
[94]		LDA	194AD+234sMCI+161pMCI+226NC	0.87	0.9	0.92	0.773
[93]	ROIs-based	KNN	192AD+229sMCI+168pMCI+229NC	0.89	0.86	0.9	0.7
[46]		SVM	198AD+238sMCI+167pMCI+231NC	0.9	0.86	0.93	0.72
[43]		Landmark detection + 3D CNN	199AD+226sMCI+167pMCI+229NC	0.91	0.88	0.94	0.77
[26]	Patch-based	Hierarchical-CNN	358AD+465sMCI+205pMCI+429NC	0.88	0.89	0.88	0.81
[30]		Attention+MIL+CNN	398AD+232sMCI+172pMCI+400NC	0.9	0.89	0.9	0.81
Proposed Method		Custom CNN	353AD+232sMCI+172pMCI+591NC	0.92	0.92	0.92	0.82

TABLE VIII

THE COMPUTATIONAL COMPLEXITY AND PARAMETERS OF PROPOSED AND MED3D METHODS

Model name	Computational complexity (Gflops)	Number of parameters	Accuracy
Med3D -10 Layer	169.55 GMac	35.47 Million	0.873
Med3D -18 Layer	253.69 GMac	63.53 Million	0.909
HFCN	240.73 GMac	37.86 Million	0.882
DA-MIDL	220.63 GMac	36.54 Million	0.904
Our Method	2.21 GMac	34.53 Million	0.920

VII. CONCLUSION

This study has proposed a patch-based convolutional network with explainable patch location suggestions for Alzheimer's Disease Diagnosis. First, we propose a fast and efficient explainable method for patch location suggestions through computing the SHapley Additive exPlanations (SHAP) contribution to a transfer learning model for AD diagnosis on massive medical data. A fast recursive partition perturbation method is introduced to effectively perturb the data to provide a fast estimation for the SHAP value of each patch. It has significantly reduced the number of patches required for achieving a good classification performance with 36 patches only, in contrast to 140 patches used in the existing statistical-based methods. Consequently, it dramatically reduces the computational complexity of the model, enabling efficient 3D data processing and analysis. Then, a novel patch-based convolutional network (sMRI-PatchNet) is designed to extract deep features of the discriminative patches and applied to AD classification and its transitional state moderate cognitive impairment (MCI) conversion prediction. The visualization results of brain regions covered by selected patches show that the proposed method can effectively identify discriminative pathological locations. These new biomarkers can help clinicians in clinical diagnosis. The classification performance and generalisability of our proposed method have been evaluated on two independent datasets and also compared with the five state-of-the-arts methods. The results show that the proposed model outperforms the existing methods and has good generalizability in all cases. Moreover, it dramatically reduces the computational complexity and computational costs, compared to traditional deep learning methods. Future research will apply this method to more medical data and related disease diagnoses.

ACKNOWLEDGMENT

This work is supported by the Royal Society - Academy of Medical Sciences Newton Advanced Fellowship (NAF\R1\180371). L.H. Han was funded by the UK Engineering and Physical Science Research Council

(EP/W007762/1) and the Small Business Research Initiative (Innovate UK, SBRI Funding Competitions: Heart Failure, Multi-morbidity and Hip Fracture).

REFERENCES

- [1] "2021 alzheimer's disease facts and figures," *Alzheimer's & Dementia: The Journal of the Alzheimer's Association*, vol. 17, no. 3, pp. 327–406, 3 2021, pMID: 33756057.
- [2] J. Rasmussen and H. Langerman, "Alzheimer's disease – why we need early diagnosis," *Degenerative Neurological and Neuromuscular Disease*, vol. 9, pp. 123–130, 12 2019, pMID: 31920420 PMCID: PMC6935598.
- [3] N. C. Fox, E. K. Warrington, and M. N. Rossor, "Serial magnetic resonance imaging of cerebral atrophy in preclinical alzheimer's disease," *The Lancet*, vol. 353, no. 9170, p. 2125, 1999, publisher: Elsevier.
- [4] W.-C. Lin, P.-L. Lee, C.-H. Lu, C.-P. Lin, and K.-H. Chou, "Linking stage-specific plasma biomarkers to gray matter atrophy in parkinson disease," *American Journal of Neuroradiology*, vol. 42, no. 8, pp. 1444–1451, 8 2021, publisher: American Journal of Neuroradiology section: Adult Brain PMID: 34045303.
- [5] K. Blennow and H. Zetterberg, "Biomarkers for alzheimer's disease: current status and prospects for the future," *Journal of Internal Medicine*, vol. 284, no. 6, pp. 643–663, 12 2018, pMID: 30051512.
- [6] G. B. Frisoni, N. C. Fox, C. R. Jack, P. Scheltens, and P. M. Thompson, "The clinical use of structural mri in alzheimer disease," *Nature Reviews Neurology*, vol. 6, no. 2, p. 67–77, 2010, publisher: Nature Publishing Group.
- [7] A. S. Lundervold and A. Lundervold, "An overview of deep learning in medical imaging focusing on mri," *Zeitschrift für Medizinische Physik*, vol. 29, no. 2, pp. 102–127, 5 2019.
- [8] P. Vemuri and C. R. Jack, "Role of structural mri in alzheimer's disease," *Alzheimer's Research & Therapy*, vol. 2, no. 4, p. 23, 8 2010.
- [9] M. R. Arbabshirani, S. Plis, J. Sui, and V. D. Calhoun, "Single subject prediction of brain disorders in neuroimaging: Promises and pitfalls," *Neuroimage*, vol. 145, p. 137–165, 2017, publisher: Elsevier.
- [10] F. Falahati, E. Westman, and A. Simmons, "Multivariate data analysis and machine learning in alzheimer's disease with a focus on structural magnetic resonance imaging," *Journal of Alzheimer's Disease*, vol. 41, no. 3, p. 685–708, 2014, publisher: IOS Press.
- [11] S. Leandrou, S. Petroudi, P. A. Kyriacou, C. C. Reyes-Aldasoro, and C. S. Pattichis, "Quantitative mri brain studies in mild cognitive impairment and alzheimer's disease: A methodological review," *IEEE Reviews in Biomedical Engineering*, vol. 11, pp. 97–111, 2018, event-title: IEEE Reviews in Biomedical Engineering.
- [12] S. Rathore, M. Habes, M. A. Ifitkhar, A. Shacklett, and C. Davatzikos, "A review on neuroimaging-based classification studies and associated feature extraction methods for alzheimer's disease and its prodromal stages," *NeuroImage*, vol. 155, pp. 530–548, 7 2017.
- [13] X. Zhang, L. Han, W. Zhu, L. Sun, and D. Zhang, "An explainable 3d residual self-attention deep neural network for joint atrophy localization and alzheimer's disease diagnosis using structural mri," *IEEE Journal of Biomedical and Health Informatics*, pp. 1–1, 2021, event-title: IEEE Journal of Biomedical and Health Informatics.
- [14] J. C. Baron, G. Chetelat, B. Desgranges, G. Perchev, B. Landeau, V. De La Sayette, and F. Eustache, "In vivo mapping of gray matter loss with voxel-based morphometry in mild alzheimer's disease," *Neuroimage*, vol. 14, no. 2, p. 298–309, 2001.
- [15] A. Khvostikov, K. Aderghal, J. Benois-Pineau, A. Krylov, and G. Catheline, "3d cnn-based classification using smri and md-dti images for alzheimer disease studies," *arXiv preprint arXiv:1801.05968*, 2018.

- [16] C. Möller, Y. A. L. Pijenburg, W. M. van der Flier, A. Versteeg, B. Tijms, J. C. de Munck, A. Hafkemeijer, S. A. R. B. Rombouts, J. van der Grond, J. van Swieten, E. Dopfer, P. Scheltens, F. Barkhof, H. Vrenken, and A. M. Wink, "Alzheimer disease and behavioral variant frontotemporal dementia: Automatic classification based on cortical atrophy for single-subject diagnosis," *Radiology*, vol. 279, no. 3, pp. 838–848, 6 2016, pMID: 26653846.
- [17] Y.-H. Kao, M.-C. Chou, C.-H. Chen, and Y.-H. Yang, "White matter changes in patients with alzheimer's disease and associated factors," *Journal of Clinical Medicine*, vol. 8, no. 2, p. 167, 2 2019, pMID: 30717182 PMID: PMC6406891.
- [18] R. Ossenkoppele, N. Mattsson, C. E. Teunissen, F. Barkhof, Y. Pijenburg, P. Scheltens, W. M. van der Flier, and G. D. Rabinovici, "Cerebrospinal fluid biomarkers and cerebral atrophy in distinct clinical variants of probable alzheimer's disease," *Neurobiology of Aging*, vol. 36, no. 8, pp. 2340–2347, 8 2015.
- [19] K. Hara, H. Kataoka, and Y. Satoh, "Can spatiotemporal 3d cnns retrace the history of 2d cnns and imagenet?" *arXiv:1711.09577 [cs]*, 4 2018, arXiv: 1711.09577. [Online]. Available: <http://arxiv.org/abs/1711.09577>
- [20] O. B. Ahmed, J. Benois-Pineau, M. Allard, C. B. Amar, G. Catheline, and A. D. N. Initiative, "Classification of alzheimer's disease subjects from mri using hippocampal visual features," *Multimedia Tools and Applications*, vol. 74, no. 4, p. 1249–1266, 2015.
- [21] O. B. Ahmed, J. Benois-Pineau, M. Allard, G. Catheline, C. B. Amar, and A. D. N. Initiative, "Recognition of alzheimer's disease and mild cognitive impairment with multimodal image-derived biomarkers and multiple kernel learning," *Neurocomputing*, vol. 220, p. 98–110, 2017.
- [22] B. Gutman, Y. Wang, J. Morra, A. W. Toga, and P. M. Thompson, "Disease classification with hippocampal shape invariants," *Hippocampus*, vol. 19, no. 6, p. 572–578, 2009.
- [23] B. Magnin, L. Mesrob, S. Kinkingnéhun, M. Pélégri-Isaac, O. Colliot, M. Sarazin, B. Dubois, S. Lehericy, and H. Benali, "Support vector machine-based classification of alzheimer's disease from whole-brain anatomical mri," *Neuroradiology*, vol. 51, no. 2, p. 73–83, 2009.
- [24] V. Planche, A. Ruet, P. Coupé, D. Lamargue-Hamel, M. Deloire, B. Pereira, J. V. Manjon, F. Munsch, N. Moscufo, and D. S. Meier, "Hippocampal microstructural damage correlates with memory impairment in clinically isolated syndrome suggestive of multiple sclerosis," *Multiple Sclerosis Journal*, vol. 23, no. 9, p. 1214–1224, 2017.
- [25] L. Wang, F. Beg, T. Ratnanather, C. Ceritoglu, L. Younes, J. C. Morris, J. G. Csernansky, and M. I. Miller, "Large deformation diffeomorphism and momentum based hippocampal shape discrimination in dementia of the alzheimer type," *IEEE transactions on medical imaging*, vol. 26, no. 4, p. 462–470, 2007, publisher: IEEE.
- [26] C. Lian, M. Liu, J. Zhang, and D. Shen, "Hierarchical fully convolutional network for joint atrophy localization and alzheimer's disease diagnosis using structural mri," *IEEE Transactions on Pattern Analysis and Machine Intelligence*, vol. 42, no. 4, pp. 880–893, 4 2020, event-title: IEEE Transactions on Pattern Analysis and Machine Intelligence.
- [27] J. Zhang, Y. Gao, Y. Gao, B. C. Munsell, and D. Shen, "Detecting anatomical landmarks for fast alzheimer's disease diagnosis," *IEEE Transactions on Medical Imaging*, vol. 35, no. 12, pp. 2524–2533, 12 2016, event-title: IEEE Transactions on Medical Imaging.
- [28] B. A. Gordon, T. Blazey, and T. L. Benzinger, "Regional variability in alzheimer's disease biomarkers," *Future neurology*, vol. 9, no. 2, pp. 131–134, 2014, pMID: 25309132 PMID: PMC4192718.
- [29] H.-I. Suk, S.-W. Lee, and D. Shen, "Hierarchical feature representation and multimodal fusion with deep learning for ad/mci diagnosis," *NeuroImage*, vol. 101, pp. 569–582, 11 2014, pMID: 25042445 PMID: PMC4165842.
- [30] W. Zhu, L. Sun, J. Huang, L. Han, and D. Zhang, "Dual attention multi-instance deep learning for alzheimer's disease diagnosis with structural mri," *IEEE Transactions on Medical Imaging*, pp. 1–1, 2021, event-title: IEEE Transactions on Medical Imaging.
- [31] S. G. Sturdevant and T. Lumley, "Statistical methods for testing carry-over effects: A mixed effects model approach," *Contemporary Clinical Trials Communications*, vol. 22, p. 100711, 6 2021.
- [32] M. Hearst, S. Dumais, E. Osuna, J. Platt, and B. Scholkopf, "Support vector machines," *IEEE Intelligent Systems and their Applications*, vol. 13, no. 4, pp. 18–28, 7 1998, event-title: IEEE Intelligent Systems and their Applications.
- [33] A. Demiriz, K. P. Bennett, and J. Shawe-Taylor, "Linear programming boosting via column generation," *Machine Learning*, vol. 46, no. 1, pp. 225–254, 1 2002.
- [34] E. Moradi, A. Pepe, C. Gaser, H. Huttunen, and J. Tohka, "Machine learning framework for early mri-based alzheimer's conversion prediction in mci subjects," *NeuroImage*, vol. 104, pp. 398–412, 1 2015.
- [35] M. F. B. Othman, N. B. Abdullah, and N. F. B. Kamal, "Mri brain classification using support vector machine," 4 2011, pp. 1–4.
- [36] Y. Zhang and S. Liu, "Analysis of structural brain mri and multi-parameter classification for alzheimer's disease," *Biomedizinische Technik. Biomedical Engineering*, vol. 63, no. 4, pp. 427–437, 7 2018, pMID: 28622141.
- [37] M. Liu, D. Zhang, and D. Shen, "Ensemble sparse classification of alzheimer's disease," *NeuroImage*, vol. 60, no. 2, pp. 1106–1116, 4 2012.
- [38] H. Wang, Z. Zhou, Y. Li, Z. Chen, P. Lu, W. Wang, W. Liu, and L. Yu, "Comparison of machine learning methods for classifying mediastinal lymph node metastasis of non-small cell lung cancer from 18f-fdg pet/ct images," *EJNMMI Research*, vol. 7, no. 1, p. 11, 12 2017.
- [39] S. Klöppel, C. M. Stonnington, C. Chu, B. Draganski, R. I. Scallan, J. D. Rohrer, N. C. Fox, C. R. Jack Jr, J. Ashburner, and R. S. Frackowiak, "Automatic classification of mr scans in alzheimer's disease," *Brain*, vol. 131, no. 3, p. 681–689, 2008, publisher: Oxford University Press.
- [40] M. Liu, D. Zhang, P.-T. Yap, and D. Shen, "Tree-guided sparse coding for brain disease classification," Springer, 2012, p. 239–247.
- [41] S. Korolev, A. Safiullin, M. Belyaev, and Y. Dodonova, "Residual and plain convolutional neural networks for 3d brain mri classification," *arXiv:1701.06643 [cs]*, 1 2017, arXiv: 1701.06643. [Online]. Available: <http://arxiv.org/abs/1701.06643>
- [42] E. Gerardin, G. Chételat, M. Chupin, R. Cuingnet, B. Desgranges, H.-S. Kim, M. Niethammer, B. Dubois, S. Lehericy, and L. Garnero, "Multi-dimensional classification of hippocampal shape features discriminates alzheimer's disease and mild cognitive impairment from normal aging," *Neuroimage*, vol. 47, no. 4, p. 1476–1486, 2009.
- [43] M. Liu, D. Zhang, D. Shen, and A. D. N. Initiative, "Hierarchical fusion of features and classifier decisions for alzheimer's disease diagnosis," *Human brain mapping*, vol. 35, no. 4, p. 1305–1319, 2014, publisher: Wiley Online Library.
- [44] K. K. Bhatia, A. Rao, A. N. Price, R. Wolz, J. V. Hajnal, and D. Rueckert, "Hierarchical manifold learning for regional image analysis," *IEEE Transactions on Medical Imaging*, vol. 33, no. 2, pp. 444–461, 2 2014, event-title: IEEE Transactions on Medical Imaging.
- [45] C. Wachinger, M. Yigitsoy, and N. Navab, "Manifold learning for image-based breathing gating with application to 4d ultrasound," Springer, 2010, p. 26–33.
- [46] T. Tong, R. Wolz, Q. Gao, R. Guerrero, J. V. Hajnal, D. Rueckert, and A. D. N. Initiative, "Multiple instance learning for classification of dementia in brain mri," *Medical image analysis*, vol. 18, no. 5, p. 808–818, 2014, publisher: Elsevier.
- [47] M. Z. Alom, T. M. Taha, C. Yakopcic, S. Westberg, P. Sidike, M. S. Nasrin, B. C. Van Esesn, A. A. S. Awwal, and V. K. Asari, "The history began from alexnet: A comprehensive survey on deep learning approaches," *arXiv:1803.01164 [cs]*, 3 2018, arXiv: 1803.01164. [Online]. Available: <http://arxiv.org/abs/1803.01164>
- [48] V. Buhrmester, D. Münch, and M. Arens, "Analysis of explainers of black box deep neural networks for computer vision: A survey," *arXiv:1911.12116 [cs]*, 11 2019, arXiv: 1911.12116. [Online]. Available: <http://arxiv.org/abs/1911.12116>
- [49] A. Das and P. Rad, "Opportunities and challenges in explainable artificial intelligence (xai): A survey," 6 2020, [Online]. Accessed 2021-10-17. [Online]. Available: <https://arxiv.org/abs/2006.11371v2>
- [50] B. H. M. van der Velden, H. J. Kuijff, K. G. A. Gilhuijs, and M. A. Viergever, "Explainable artificial intelligence (xai) in deep learning-based medical image analysis," *Medical Image Analysis*, vol. 79, p. 102470, 7 2022.
- [51] R. R. Selvaraju, M. Cogswell, A. Das, R. Vedantam, D. Parikh, and D. Batra, "Grad-cam: Visual explanations from deep networks via gradient-based localization," *arXiv:1610.02391 [cs]*, 10 2016, arXiv: 1610.02391. [Online]. Available: <http://arxiv.org/abs/1610.02391>
- [52] K. Simonyan, A. Vedaldi, and A. Zisserman, "Deep inside convolutional networks: Visualising image classification models and saliency maps," *arXiv:1312.6034 [cs]*, 12 2013, arXiv: 1312.6034. [Online]. Available: <http://arxiv.org/abs/1312.6034>
- [53] J. T. Springenberg, A. Dosovitskiy, T. Brox, and M. Riedmiller, "Striving for simplicity: The all convolutional net," *arXiv:1412.6806 [cs]*, 12 2014, arXiv: 1412.6806. [Online]. Available: <http://arxiv.org/abs/1412.6806>
- [54] B. Zhou, A. Khosla, A. Lapedriza, A. Oliva, and A. Torralba, "Learning deep features for discriminative localization," Las Vegas, NV, USA: IEEE, 6 2016, pp. 2921–2929, [Online]. Accessed 2019-05-11. [Online]. Available: <http://ieeexplore.ieee.org/document/7780688/>
- [55] J. Adebayo, J. Gilmer, M. Muelly, I. Goodfellow, M. Hardt, and B. Kim, "Sanity checks for saliency maps," *arXiv:1810.03292 [cs, stat]*, 10 2018, arXiv: 1810.03292. [Online]. Available: <http://arxiv.org/abs/1810.03292>

- [56] A. Ghorbani, A. Abid, and J. Zou, "Interpretation of neural networks is fragile," *arXiv:1710.10547 [cs, stat]*, 11 2018, arXiv: 1710.10547. [Online]. Available: <http://arxiv.org/abs/1710.10547>
- [57] P.-J. Kindermans, S. Hooker, J. Adebayo, M. Alber, K. T. Schütt, S. Dähne, D. Erhan, and B. Kim, "The (un) reliability of saliency methods," in *Explainable AI: Interpreting, Explaining and Visualizing Deep Learning*. Springer, 2019, pp. 267–280.
- [58] I. Covert, S. Lundberg, and S.-I. Lee, "Explaining by removing: A unified framework for model explanation," *arXiv:2011.14878 [cs, stat]*, 11 2020, arXiv: 2011.14878. [Online]. Available: <http://arxiv.org/abs/2011.14878>
- [59] M. T. Ribeiro, S. Singh, and C. Guestrin, "'why should i trust you?': Explaining the predictions of any classifier," *arXiv:1602.04938 [cs, stat]*, 2 2016, arXiv: 1602.04938. [Online]. Available: <http://arxiv.org/abs/1602.04938>
- [60] L. S. Shapley, "Notes on the n-person game—ii: The value of an n-person game, the rand corporation, the rand corporation," *Research Memorandum*, vol. 670, 1951.
- [61] S. M. Lundberg and S.-I. Lee, "A unified approach to interpreting model predictions," *Advances in neural information processing systems*, vol. 30, 2017.
- [62] A. Khakzar, S. Baselizadeh, S. Khanduja, C. Rupprecht, S. T. Kim, and N. Navab, "Improving feature attribution through input-specific network pruning," *arXiv preprint arXiv:1911.11081*, 2019.
- [63] S. Chen, K. Ma, and Y. Zheng, "Med3d: Transfer learning for 3d medical image analysis," *arXiv:1904.00625 [cs]*, 7 2019, arXiv: 1904.00625. [Online]. Available: <http://arxiv.org/abs/1904.00625>
- [64] A. Dosovitskiy, L. Beyer, A. Kolesnikov, D. Weissenborn, X. Zhai, T. Unterthiner, M. Dehghani, M. Minderer, G. Heigold, S. Gelly, J. Uszkoreit, and N. Houlsby, "An image is worth 16x16 words: Transformers for image recognition at scale," *arXiv:2010.11929 [cs]*, 10 2020, arXiv: 2010.11929. [Online]. Available: <http://arxiv.org/abs/2010.11929>
- [65] G. E. Hinton, "Rectified linear units improve restricted boltzmann machines vinod nair," 2010.
- [66] S. Ioffe and C. Szegedy, "Batch normalization: Accelerating deep network training by reducing internal covariate shift," *arXiv:1502.03167 [cs]*, 2 2015, arXiv: 1502.03167. [Online]. Available: <http://arxiv.org/abs/1502.03167>
- [67] K. He, X. Zhang, S. Ren, and J. Sun, "Deep residual learning for image recognition," *arXiv:1512.03385 [cs]*, 12 2015, arXiv: 1512.03385. [Online]. Available: <http://arxiv.org/abs/1512.03385>
- [68] J. G. Sled, A. P. Zijdenbos, and A. C. Evans, "A nonparametric method for automatic correction of intensity nonuniformity in mri data," *IEEE transactions on medical imaging*, vol. 17, no. 1, pp. 87–97, 2 1998, pMID: 9617910.
- [69] Y. Wang, J. Nie, P.-T. Yap, F. Shi, L. Guo, and D. Shen, "Robust deformable-surface-based skull-stripping for large-scale studies," ser. Lecture Notes in Computer Science, G. Fichtinger, A. Martel, and T. Peters, Eds. Berlin, Heidelberg: Springer, 2011, pp. 635–642.
- [70] C. J. Holmes, R. Hoge, L. Collins, R. Woods, A. W. Toga, and A. C. Evans, "Enhancement of mr images using registration for signal averaging," *Journal of Computer Assisted Tomography*, vol. 22, no. 2, pp. 324–333, 4 1998, pMID: 9530404.
- [71] J. Ashburner and K. J. Friston, "Voxel-based morphometry—the methods," *NeuroImage*, vol. 11, no. 6, pp. 805–821, 6 2000.
- [72] D. Zhang, Y. Wang, L. Zhou, H. Yuan, D. Shen, and A. D. N. Initiative, "Multimodal classification of alzheimer's disease and mild cognitive impairment," *Neuroimage*, vol. 55, no. 3, p. 856–867, 2011.
- [73] D. Shen and C. Davatzikos, "Hammer: hierarchical attribute matching mechanism for elastic registration," *IEEE transactions on medical imaging*, vol. 21, no. 11, p. 1421–1439, 2002, publisher: IEEE.
- [74] N. J. Kabani, D. J. MacDonald, C. J. Holmes, and A. C. Evans, "3d anatomical atlas of the human brain," *NeuroImage*, vol. 7, no. 4, p. S717, 1998, publisher: Elsevier.
- [75] G. Ke, Q. Meng, T. Finley, T. Wang, W. Chen, W. Ma, Q. Ye, and T.-Y. Liu, "Lightgbm: A highly efficient gradient boosting decision tree," *Advances in neural information processing systems*, vol. 30, p. 3146–3154, 2017.
- [76] D. Kingma and J. Ba, "Adam: A method for stochastic optimization," *Computer Science*, 2014.
- [77] d. P.-T. Boer, D. Kroese, S. Mannor, and R. Y. Rubinstein, "A tutorial on the cross-entropy method," *Annals of operations research*, vol. 134, no. 1, pp. 19–67, 1 2005.
- [78] T. K. Kim, "T test as a parametric statistic," *Korean Journal of Anesthesiology*, vol. 68, no. 6, pp. 540–546, 12 2015, pMID: 26634076 PMCID: PMC4667138.
- [79] R. Craig-Schapiro, A. M. Fagan, and D. M. Holtzman, "Biomarkers of alzheimer's disease," *Neurobiology of disease*, vol. 35, no. 2, p. 128–140, 2009, publisher: Elsevier.
- [80] C. Humpel, "Identifying and validating biomarkers for alzheimer's disease," *Trends in biotechnology*, vol. 29, no. 1, p. 26–32, 2011, publisher: Elsevier.
- [81] E. T. Rolls, C.-C. Huang, C.-P. Lin, J. Feng, and M. Joliot, "Automated anatomical labelling atlas 3," *NeuroImage*, vol. 206, p. 116189, 2 2020.
- [82] H. Yang, H. Xu, Q. Li, Y. Jin, W. Jiang, J. Wang, Y. Wu, W. Li, C. Yang, X. Li, S. Xiao, F. Shi, and T. Wang, "Study of brain morphology change in alzheimer's disease and amnesic mild cognitive impairment compared with normal controls," *General Psychiatry*, vol. 32, no. 2, p. e100005, 4 2019, pMID: 31179429 PMCID: PMC6551438.
- [83] E. D. Vidoni, G. P. Thomas, R. A. Honea, N. Loskutova, and J. M. Burns, "Evidence of altered corticomotor system connectivity in early-stage alzheimer's disease," *Journal of Neurologic Physical Therapy*, vol. 36, no. 1, pp. 8–16, 3 2012, pMID: 22333920 PMCID: PMC3288781.
- [84] C. Murphy, "Olfactory and other sensory impairments in alzheimer disease," *Nature Reviews Neurology*, vol. 15, no. 1, pp. 11–24, 2019.
- [85] J. Chen, X. Duan, H. Shu, Z. Wang, Z. Long, D. Liu, W. Liao, Y. Shi, H. Chen, and Z. Zhang, "Differential contributions of subregions of medial temporal lobe to memory system in amnesic mild cognitive impairment: insights from fmri study," *Scientific reports*, vol. 6, no. 1, pp. 1–14, 2016.
- [86] A. L. Foundas, C. M. Leonard, S. M. Mahoney, O. F. Agee, and K. M. Heilman, "Atrophy of the hippocampus, parietal cortex, and insula in alzheimer's disease: a volumetric magnetic resonance imaging study," *Neuropsychiatry, Neuropsychology, and Behavioral Neurology*, vol. 10, no. 2, pp. 81–89, 4 1997, pMID: 9150507.
- [87] X. Liu, W. Chen, H. Hou, X. Chen, J. Zhang, J. Liu, Z. Guo, and G. Bai, "Decreased functional connectivity between the dorsal anterior cingulate cortex and lingual gyrus in alzheimer's disease patients with depression," *Behavioural Brain Research*, vol. 326, pp. 132–138, 5 2017, pMID: 28126471.
- [88] P. T. Nelson, E. L. Abner, S. W. Scheff, F. A. Schmitt, R. J. Kryscio, G. A. Jicha, C. D. Smith, E. Patel, and W. R. Markesbery, "Alzheimer's-type neuropathology in the precuneus is not increased relative to other areas of neocortex across a range of cognitive impairment," *Neuroscience letters*, vol. 450, no. 3, pp. 336–339, 2 2009, pMID: 19010392 PMCID: PMC2839166.
- [89] K. Persson, V. Bohbot, N. Bogdanovic, G. Selbæk, A. Brækhus, and K. Engedal, "Finding of increased caudate nucleus in patients with alzheimer's disease," *Acta Neurologica Scandinavica*, vol. 137, no. 2, pp. 224–232, 2018.
- [90] S. P. Poulin, R. Dautoff, J. C. Morris, L. F. Barrett, and B. C. Dickerson, "Amygdala atrophy is prominent in early alzheimer's disease and relates to symptom severity," *Psychiatry research*, vol. 194, no. 1, pp. 7–13, 10 2011, pMID: 21920712 PMCID: PMC3185127.
- [91] J. P. Aggleton, A. Pralus, A. J. D. Nelson, and M. Hornberger, "Thalamic pathology and memory loss in early alzheimer's disease: moving the focus from the medial temporal lobe to papez circuit," *Brain: A Journal of Neurology*, vol. 139, no. Pt 7, pp. 1877–1890, 7 2016, pMID: 27190025 PMCID: PMC4939698.
- [92] R. Cuingnet, E. Gerardin, J. Tessieras, G. Auzias, S. Lehericy, M.-O. Habert, M. Chupin, H. Benali, and O. Colliot, "Automatic classification of patients with alzheimer's disease from structural mri: A comparison of ten methods using the adni database," *NeuroImage*, vol. 56, no. 2, pp. 766–781, 5 2011.
- [93] P. Cao, X. Liu, J. Yang, D. Zhao, M. Huang, J. Zhang, and O. Zaiane, "Nonlinearity-aware based dimensionality reduction and over-sampling for ad/mci classification from mri measures," *Computers in biology and medicine*, vol. 91, p. 21–37, 2017, publisher: Elsevier.
- [94] S. F. Eskildsen, P. Coupé, D. García-Lorenzo, V. Fonov, J. C. Pruessner, D. L. Collins, and A. D. N. Initiative, "Prediction of alzheimer's disease in subjects with mild cognitive impairment from the adni cohort using patterns of cortical thinning," *Neuroimage*, vol. 65, p. 511–521, 2013, publisher: Elsevier.